Midbrain encodes sound detection behavior without auditory cortex

Tai-Ying Lee, Yves Weissenberger, Andrew J King, Johannes C Dahmen

Department of Physiology, Anatomy and Genetics, University of Oxford, Oxford, United Kingdom

Correspondence should be addressed to J.C.D. (johannes.dahmen@dpag.ox.ac.uk).

Abstract

Hearing involves analyzing the physical attributes of sounds and integrating the results of this analysis with other sensory, cognitive and motor variables in order to guide adaptive behavior. The auditory cortex is considered crucial for the integration of acoustic and contextual information and is thought to share the resulting representations with subcortical auditory structures via its vast descending projections. By imaging cellular activity in the corticorecipient shell of the inferior colliculus of mice engaged in a sound detection task, we show that the majority of neurons encode information beyond the physical attributes of the stimulus and that the animals' behavior can be decoded from the activity of those neurons with a high degree of accuracy. Surprisingly, this was also the case in mice in which auditory cortical input to the midbrain had been removed by bilateral cortical lesions. This illustrates that subcortical auditory structures have access to a wealth of non-acoustic information and can, independently of the auditory cortex, carry much richer neural representations than previously thought.

Introduction

Classically, perception is considered to rely on the flow of information from the sensory periphery via a sequence of hierarchically-organized brain structures up to the cortex. The ascending sensory pathways connecting these structures have been studied extensively and much has been learned about how signals are relayed, how features are extracted, and how information is integrated to produce increasingly abstract representations of the sensory environment. These pathways are paralleled by descending pathways that can feed information back to lower-order sensory structures. The fact that descending projections often outnumber their feedforward counterparts (Sherman, 2007) attests to their likely importance for brain function. This may include turning an otherwise passive, stimulus-driven device into an active and adaptive brain that is capable of processing sensory input within its behavioral context and, therefore, able to learn and create meaning (Engel et al., 2001; Kraus and White-Schwoch, 2015; Malmierca, Anderson and Antunes, 2015).

The descending projections of the auditory cortex target all major subcortical stations of the auditory pathway and are among the largest pathways of the brain (Winer, 2006; Bajo and King, 2013; Antunes and Malmierca, 2021), making them a particularly suitable system for investigating the behavioral and physiological consequences of corticofugal processing. One of their main targets is the inferior colliculus (IC), an obligatory midbrain relay for nearly all ascending auditory input. The corticocollicular projection primarily terminates in the non-lemniscal shell of the IC. The shell encapsulates and is extensively connected with the central nucleus of the IC, which forms part of the tonotopically organized core or lemniscal auditory pathway to the primary auditory cortex. The projection from the auditory cortex to the midbrain was identified almost a century ago (Mettler 1935) and decades of research have since demonstrated that manipulating the activity of descending projection neurons can alter the collicular representations of multiple sound features, influence adaptive plasticity and perceptual learning, and even trigger an innate flight response (Suga 2008; Nakamoto et al 2008; Bajo et al 2010; Xion et al 2015; Blackwell et al 2020). However, experimental evidence, especially from behaving animals, that could help explain what information the auditory midbrain and other subcortical sensory structures rely on their cortical input for is still very limited.

Interactions between different sensory pathways occur at multiple processing levels and they are also closely linked with the brain's motor centers and neuromodulatory regions. Indeed, recordings in awake animals have shown that behavior, cognition and brain state can strongly influence activity in the sensory pathways (Schneider and Mooney, 2018; McCormick et al., 2020; Parker et al., 2020). Consistent with a hierarchical view of sensory processing in which neurons at higher levels carry progressively more complex representations of the world, such contextual influences appear particularly strong in the cortex (Stringer et al,. 2019; Musall et al., 2019) and may to a large extent be the result of intracortical processing (Noudoost et al., 2010; Schneider et al., 2014; Song et al., 2017). Nevertheless, non-acoustic and contextual variables can also alter sensory processing at subcortical levels, including the IC and particularly its shell (Metzger et al., 2006; Gruters and Groh, 2012; Chen and Song, 2019; Yang et al., 2020; Parras et al., 2017; Saderi et al., 2021). This raises the possibility that these context-dependent effects may be inherited from the auditory cortex.

To test whether auditory midbrain neurons convey behaviorally-relevant signals that depend on descending cortical inputs, we imaged corticorecipient IC shell neurons in mice engaged in a sound detection task. We found that the activity of most neurons contained information beyond the physical attributes of the sound and that this information could be used to decode the animals' behavior with a high degree of accuracy. Surprisingly, this was the case both in

mice with an intact cortex and those in which the auditory cortex had been lesioned. These findings suggest that subcortical auditory structures have access to a wealth of non-auditory information independently of descending inputs from the auditory cortex. Consequently, the contextually-enriched representations that are characteristic of sensory cortices can arise from subcortical processing.

Results

Transient suppression of the auditory cortex impairs sound detection. Our aim was to characterize the activity of neurons in the shell of the IC in animals engaged in sound-guided behavior and assess how this activity is influenced by the input from the auditory cortex. To this end, we trained water-regulated mice on a sound detection task (Figure 1A) in which they were rewarded with a drop of water for licking in response to a click sound. Transient pharmacological silencing of auditory cortex using the GABA-A agonist muscimol has been shown to abolish the ability of rodents (Talwar et al., 2001), including head-fixed mice (Li et al., 2017), to perform a sound detection task, making this approach unsuitable for our aim of exploring the role of IC during behavior. We found that optogenetic suppression of cortical activity by photoactivating ChR2-expressing inhibitory neurons in *GAD2-IRES-cre* mice (Lohse et al., 2020) also significantly impaired sound detection performance (d': 1.51 ± 0.71 vs 1.10 ± 1.18 (median ± interquartile range); p = 0.0009; Wilcoxon signed rank test; Figure 1B,C), albeit not to the same degree as pharmacological silencing. Optogenetic suppression of cortical activity is thus also unsuitable for this study as it would leave us unable to determine whether any changes in the activity of IC neurons arise from removal of their auditory cortical input or are a consequence of alterations in the animals' behavior.

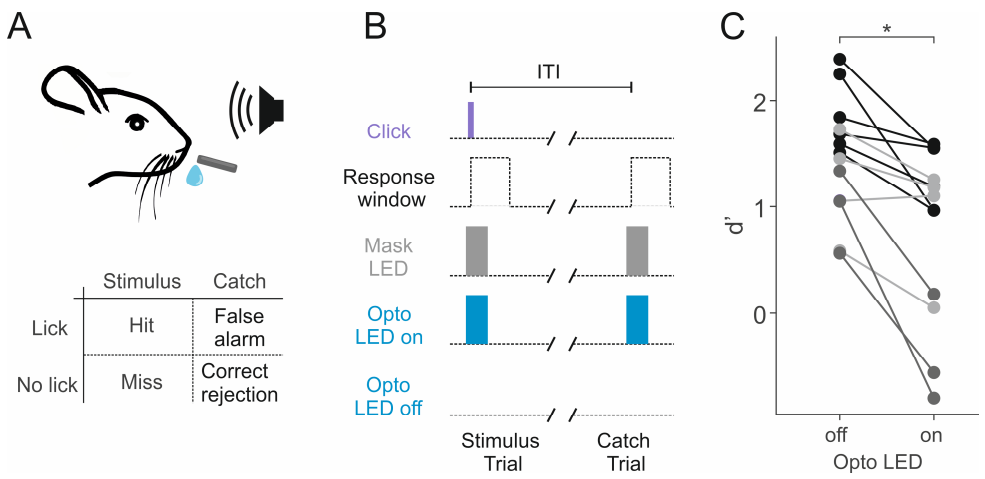

Figure 1. Optogenetic inactivation of auditory cortex impairs sound detection performance in head-fixed mice. (**A**) Schematic of the click detection task. (**B**) Trial structure for experiments involving optogenetic manipulation. Stimulus trials (click) and catch trials (no click) were randomly interleaved and consecutive trials separated by a randomly varying inter-trial interval (ITI). LEDs placed over each auditory cortex were switched on randomly in half of the stimulus and catch trials to photoactivate the opsin. A separate set of LEDs (Mask LEDs) placed directly in front of the mouse's eyes were switched on in all Opto-on and Opto-off trials to prevent mice from visually registering the light from the photoactivation LEDs. **c** Detection performance in trials during which light was shone on the auditory cortex for optogenetic silencing (Opto LED – on) vs control trials (Opto LED - off). Each data point indicates the 'd prime' obtained on a single day for a single mouse. Different shades of gray indicate different mice (n = 3).

Auditory cortex lesions leave detection ability intact. Several recent studies have shown that in contrast to the disruptive effects of transient silencing, cortical lesions leave performance in some sensory tasks intact (Hong et al., 2018; Ceballo et al., 2019; O'Sullivan et al., 2019). In order to compare how auditory cortex lesions impact sound detection performance, we therefore lesioned the auditory cortex bilaterally in 7 out of 16 animals.

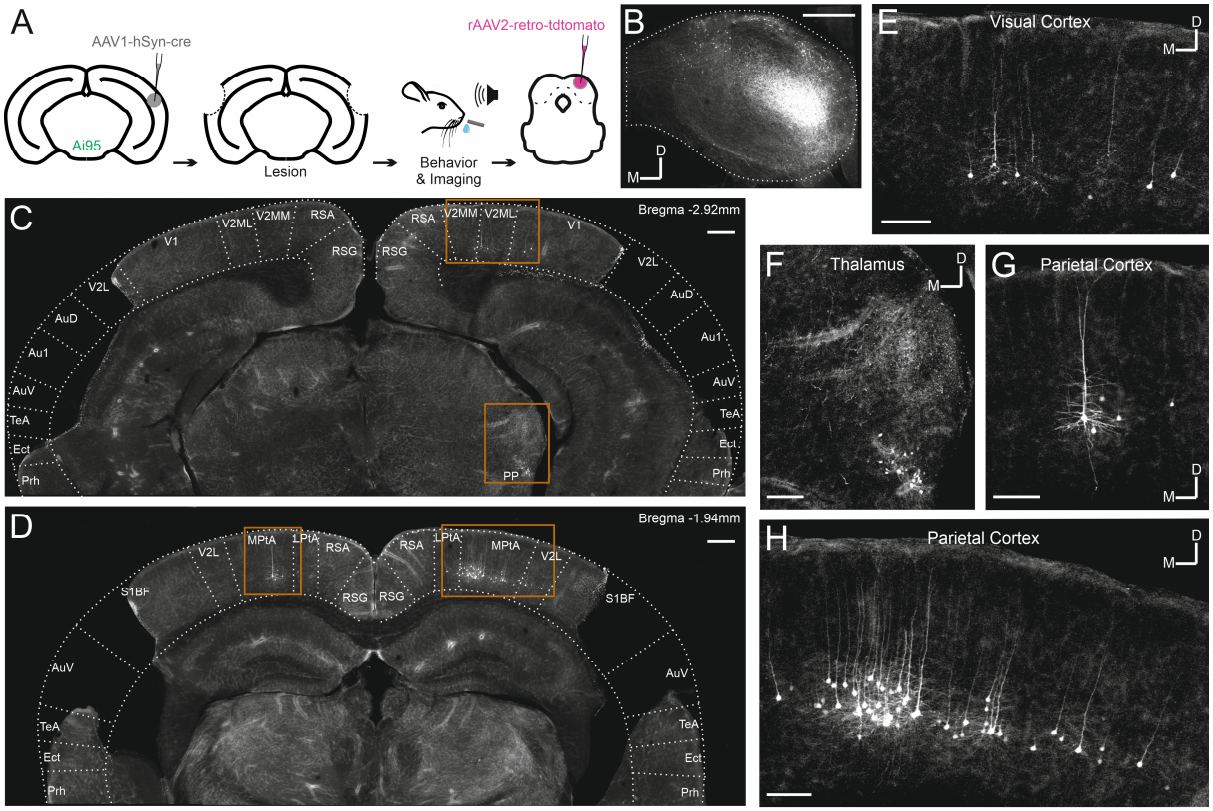

Figure 2. Retrograde viral tracing of IC-projecting neurons in bilaterally lesioned mice. (**A**) Timeline of experimental procedures. AAV1.hSyn.cre.WPRE was injected into the right auditory cortex of GCaMP6f reporter (Ai95D) mice. This causes transsynaptic delivery of the virus to the IC and expression of GCaMP6f in corticorecipient IC neurons. Several weeks later the mice underwent bilateral lesioning of auditory cortex either by aspiration or by thermocoagulation (see Figure 2 - figure supplement 2 for histological sections from a mouse that underwent thermocoagulation) and were implanted with a glass window over the right auditory cortex. Following recovery from this procedure, water access was restricted and, 2-3 days later, behavioral training and imaging commenced. After data collection had been completed, rAAV2-retro-tdTomato was injected in the dorsal IC in order to label corticocollicular neurons that had remained intact. (**B**) Coronal section of the right IC showing tdTomato-labeled neurons. A total of 150 nL of rAAV2-retro-tdTomato was injected across three different sites and depths of about 100 µm – 400 µm below the brain surface. The large bright spot comprises retrogradely-labelled neurons in the central nucleus of the IC. Scale bar, 500 µm. (**C**,**D**) Coronal sections showing lesion extent at different rostro-caudal positions for one example mouse. Area borders were drawn onto the images according to Paxinos and Franklin (2001). No retrogradely-labeled neurons were found near the lesion borders, suggesting that the auditory cortex had been completely removed. Corticocollicular projections from non-temporal regions as well as thalamocollicular projections remained intact. Scale bars, 200 µm. (**E**) High magnification image (location shown by the upper rectangle in **C**) showing corticocollicular neurons in visual cortex. Scale bar, 100 µm. (**F**) High magnification image (location shown by the lower rectangle in **C**) showing thalamocollicular neurons in the peripeduncular nucleus of the thalamus (PP). Scale bar, 100 µm. (**G,H)** High magnification images (locations shown by the left and right rectangles in **D**, respectively) showing corticocollicular neurons in the parietal cortex. Scale bars,100 µm. Cortical area abbreviations: Au1, primary auditory; AuD, secondary auditory, dorsal; AuV, secondary auditory, ventral; Ect, ectorhinal; LPta, lateral parietal association; MPta, medial parietal association; Prh, perirhinal; RSG, retrosplenial granular; RSA, retrosplenial agranular; S1BF, primary somatosensory, barrel field; TeA, temporal association; V1, primary visual; V2L, secondary visual, lateral; V2ML, secondary visual mediolateral; V2MM, secondary visual mediomedial.

Most corticocollicular neurons project ipsilaterally, with a substantial proportion also sending axons to the contralateral midbrain (Stebbings et al., 2014). The majority of corticocollicular neurons are found in the temporal cortex, and overwhelmingly in the auditory fields, while a small fraction populates adjacent areas, such as the temporal association area (Figure 2 - figure supplement 1). After the experiments, we injected a retrogradely-transported viral tracer (rAAV2-retro-tdTomato) into the right IC to determine whether any corticocollicular neurons remained after the AC lesions (Figure 2).

Lesioned mice were able to learn and perform the click detection task. In fact, there was no significant difference between them and the non-lesioned mice in their learning speed (Figure 3A, $p > 0.05$, mixed-design ANOVAs) and psychometric functions (Figure 3B, $p > 0.05$, mixed-design ANOVA). Cortical lesioning thus leaves behavioral sensitivity to clicks intact and therefore provides a means of examining the effects of removing corticocollicular input, albeit non-reversibly, without directly affecting sound detection performance.

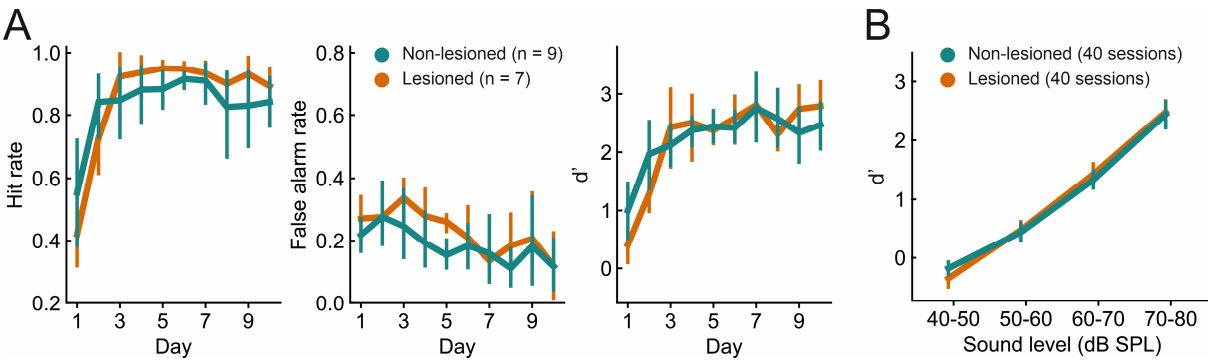

Figure 3. Lesioned and non-lesioned mice are indistinguishable in their click detection learning rate and sensitivity. (**A**) Hit rate, false alarm rate and d' over time for lesioned and non-lesioned animals. (**B**) d' as a function of sound level. The sound levels used were not identical across all mice and were therefore combined into 10-dB wide bins. Error bars indicate 95% confidence intervals.

Transsynaptic labeling and two-photon calcium imaging of auditory corticorecipient IC neurons. Manipulations of auditory cortical activity can influence the activity of neurons throughout the IC, including the central nucleus (Suga 2008, Nakamoto et al., 2008), where corticocollicular axons are relatively sparse (Stebbings et al 2014). The strongest effects, however, tend to be observed in the shell, where cortical input is densest (Nakamoto et al., 2008; Vila et al 2019; Blackwell et al., 2020). But even here, effects can be subtle (Vila et al., 2019) or undetectable (Blackwell et al., 2020) especially for cortical silencing. It is also unclear whether the IC neurons recorded in these studies receive cortical input or not. Therefore, we took a projection-specific approach to record the activity of IC neurons that receive direct input from the auditory cortex. More specifically, we injected AAV1.hSyn.Cre.WPRE, a virus with anterograde transsynaptic spread properties (Zingg et al., 2017), into the right auditory cortex of, initially, a tdTomato (Ai9) reporter mouse. This resulted in the expression of cre-recombinase and the reporter gene in neurons that receive input from the auditory cortex, including the corticorecipient neurons of the IC (Figure 4A). By employing this approach in GCaMP6f (Ai95D) reporter mice, we could target the expression of a calcium indicator to corticorecipient IC neurons and then proceed to record the activity of those neurons using two-photon microscopy (Figure 4B).

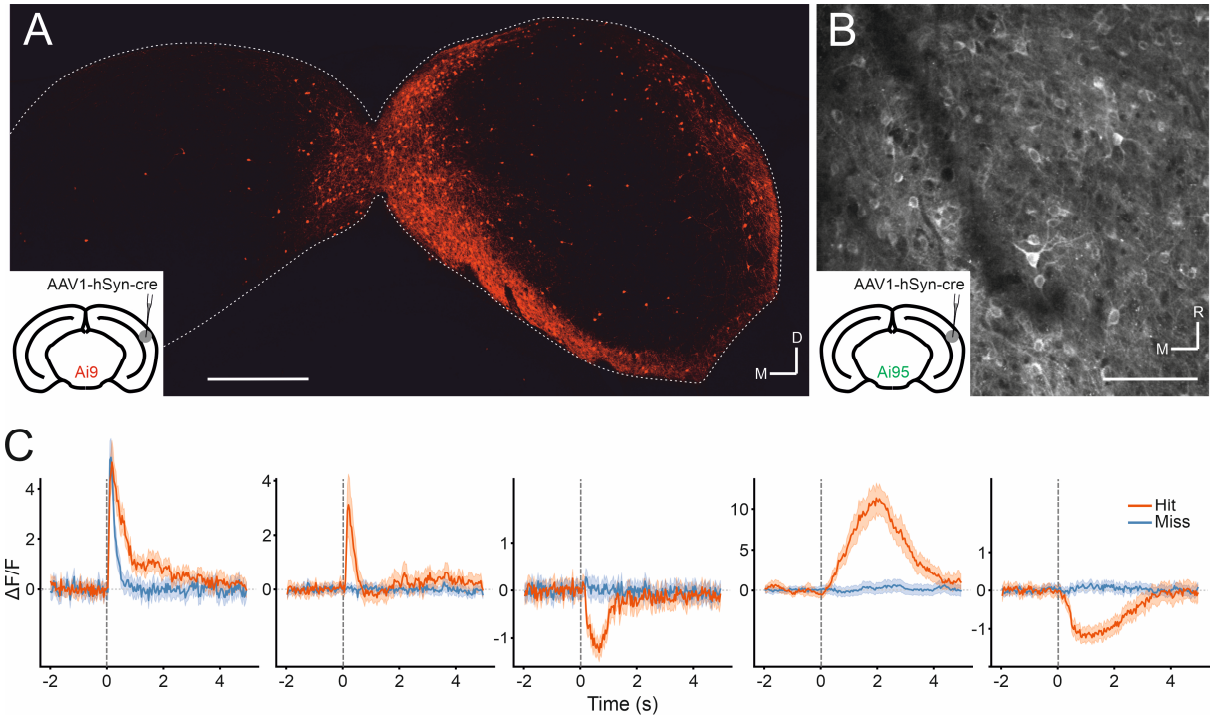

Figure 4. Transsynaptic targeting and two-photon calcium imaging of corticorecipient IC shell neurons. (**A**) Coronal section of the left and right IC of a tdTomato-reporter (Ai9) mouse in which AAV1.hSyn.Cre.WPRE had been injected into the right auditory cortex three weeks before perfusion. The transsynaptically transported virus drove expression of cre-recombinase and tdTomato in neurons that receive input from the auditory cortex, including the corticorecipient neurons in the IC. tdTomato-labeled neurons were predominantly found in the shell of the ipsilateral (right) IC. Scale bar, 500 µm. (**B**) In vivo two-photon imaging field of view taken approximately 100 µm below the dorsal surface of the right IC of a GCaMP6f-reporter mouse (Ai95D) in which GCaMP6f expression had been driven in corticorecipient IC neurons by injection of AAV1.hSyn.Cre.WPRE into the right auditory cortex. Scale bar, 100 µm. (**C**) Example average response profiles of five corticorecipient IC neurons for different trial outcomes. Error bars represent 95% confidence intervals.

Corticorecipient IC neurons display heterogeneous response profiles. The activity of individual corticorecipient IC neurons showed distinct response profiles across neurons and trial outcomes (hit vs miss) (Figure 4C). To capture the heterogeneity of response patterns across all recorded neurons, we used an unsupervised clustering algorithm (Namboodiri et al. 2019) to group the average responses of hit and miss trials for each neuron. This yielded 10 clusters that displayed different response patterns over the course of the trial (Figure 5A, B). Remarkably, most of the clusters exhibited distinct activity for hit vs miss trials. Some hit trial profiles were characterized by increases or decreases in activity, with a very sharp, short-latency onset, as in clusters 4 and 10 (see Figure 5 - figure supplement 1 for a scaled version of cluster 10), and others by much more gradual changes in which a peak occurred seconds after the trial onset, as in clusters 5 and 9. Cluster 3, which contained the smallest number of neurons, was an exception in that it showed a transient, short latency response to the stimulus for both trial outcomes. The response profiles of some other clusters, especially clusters 6 and 8, were also qualitatively similar across hit and miss trials and/or only weakly modulated across both trial types.

This suggests that the activity of the majority of neurons in the recorded population contained information beyond the physical properties of the stimulus. Given that licking causes self-generated sounds, IC neurons could, in principle, respond to the sound of licking. However,

given how quiet these are - estimated to be just 12 dB SPL (Singla et al., 2017) - and that much of the response to such lick-related sounds is already canceled out at the level of the cochlear nucleus (Singla et al., 2017), it is highly unlikely that lick-related sounds play a major role in driving activity in the IC.

To assess whether certain response profiles depended on auditory cortical input, we compared the ratio of neurons from lesioned vs non-lesioned mice in each cluster to that of the overall recorded population. The number of recorded neurons was unequal for lesioned and non-lesioned mice (952 vs 1697, respectively), reflecting the fact that a greater proportion of imaging sessions in non-lesioned animals were carried out using a larger field of view, which contained larger numbers of neurons (Figure 5 - figure supplement 2). To account for this, the percentages shown on the pie charts were normalized to the ratio in the overall population (Figure 5C). Neurons from both groups were well represented across all 10 clusters and while a significant difference in the lesioned/non-lesioned ratio was found for four clusters, only one deviated from a 50/50 split by more than 10%. This suggests that in mice engaged in a sound detection task, the activity of the neurons was broadly consistent in lesioned and non-lesioned animals and therefore that the IC shell can produce very similar output regardless of whether auditory cortical input is available or not.

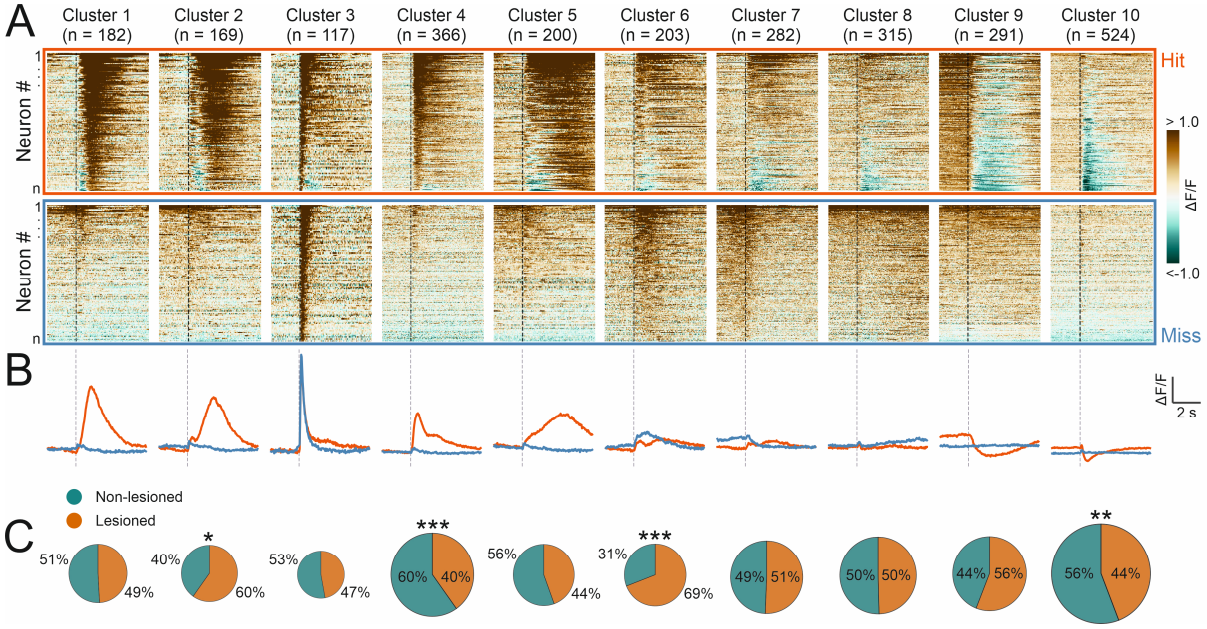

Fig. 5 Corticorecipient IC neurons display heterogeneous response profiles. (**A**) Peri-stimulus time histograms for all neurons in the dataset separated by cluster identity: hit trials (top) vs miss trials (bottom). (**B**) Averaged response profiles obtained by taking the mean across all neurons in a cluster separately for hit (red) and miss (blue) trials. (**C**) Pie charts illustrating the proportion of neurons from lesioned and non-lesioned mice in each cluster. The size of each pie chart is proportional to the total number of neurons in each cluster. Given the unequal number of neurons from lesioned (952 neurons) and non-lesioned (1697 neurons) mice, the pie charts were normalized to the overall sample size such that a 50/50 split indicates a lesioned/non-lesioned distribution that is identical to that of the overall population. Asterisks indicate a significant difference between the lesioned/non-lesioned distribution in the given cluster and that in the overall population. *: $p < 0.05$, **: < 0.01, ***: $p < 0.001$, two-sided one proportion Z-test.

Behavior can be accurately decoded from neural activity in lesioned and non-lesioned mice. The average responses of individual neurons in the IC shell exhibited a variety of activity patterns associated with both the stimulus and the trial outcome (Figure 5A,B). To gain insight into how these activity patterns can be read out collectively on a trial-by-trial basis, we assessed the relationship between the trial-by-trial network activity and the trial outcome. We trained logistic regression models to classify hit vs miss trials on a trial-by-trial, frame-by-frame basis. As different populations of neurons were recorded in different imaging sessions, the models were trained separately for each session. “Dummy models”, which randomly classified trials while taking into account the probability of hit vs miss trials in a given session, were used as the baseline model performance. If the population activity of the IC shell contained information about the trial outcome, the performance of the models would be significantly above baseline.

In both lesioned and non-lesioned mice, the average model performance was significantly above baseline in classifying hit vs miss trials ($p < 0.05$, one-sided Wilcoxon signed-rank test or paired t-test with Bonferroni correction, Figure 6A) and showed a temporal profile that is consistent with the dynamics of the activity profiles of some of the clusters, in particular clusters 1, 2, 4, 5, 9, 10 (Figure 5A,B). Additionally, the model performance in non-lesioned mice was significantly better than that in lesioned mice ($p < 0.05$, one-sided Mann-Whitney U test or t-test with Bonferroni correction, Figure 6A). The difference in the decoding performance was not the result of the difference in the number of neurons between non-lesioned and lesioned mice (Figure 6 - figure supplement 1).

By examining the corticocollicular labeling and referencing the histological sections against a mouse brain atlas (Paxinos and Franklin, 2001), we categorized the mice according to lesion size. Four of the seven lesioned animals had “(near-)complete” lesions, meaning that all (Figure 2) or an estimated ~95% (Figure 2 - figure supplement 2) of the auditory cortex had been lesioned, while the remaining mice had “partial” lesions, with an estimated 15% - 25% of the auditory cortex left intact. To assess whether the size of the lesions impacted the decoding performance, we compared the model performance between mice that had (near-)complete lesions and mice that had partial lesions. This revealed that the average decoding performance for mice with (near-)complete lesions was significantly better than that measured for mice with partial lesions. While this pattern of results may be unexpected, it is consistent with work showing smaller lesions being associated with greater somatosensory processing deficits (Hong et al., 2018). Additionally, the decoding performance in mice with (near-)complete lesions was largely indistinguishable from that in mice with an intact auditory cortex, implying that the population activity of IC shell neurons can contain similar amounts of information about the animal’s behavior regardless of whether descending input from the cortex is available or not (Figure 6B).

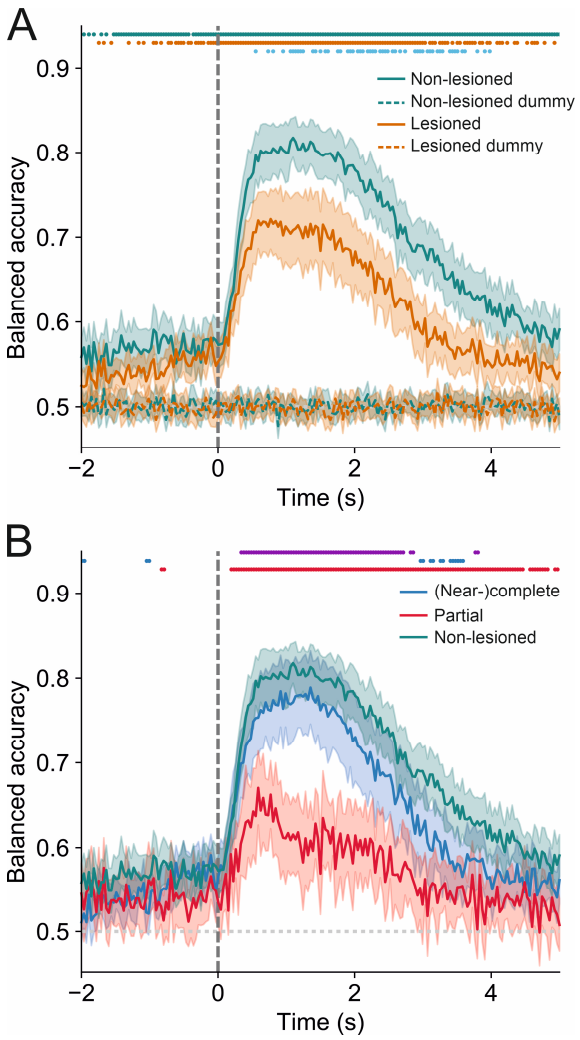

Figure 6. Trial outcome can be accurately decoded from neural activity in lesioned and non-lesioned mice. (**A**) Average decoding accuracy of logistic regression models as a function of time against dummy models with a score of 0.5 meaning chance performance and a score of 1 being the maximum. Data shown depict the mean model accuracy across 37 (lesioned) and 38 (non-lesioned) sessions, respectively. Dots at the top indicate the timepoints (frames) where the model performance was significantly different between trained and dummy models for non-lesioned mice (teal) or lesioned mice (orange) ($p < 0.05$, one-sided Wilcoxon signed-rank test or paired t-test with Bonferroni correction, depending on whether normality assumption was met), and between the trained models for non-lesioned vs lesioned mice (blue) ($p < 0.05$, one-sided Mann-Whitney U test or t-test with Bonferroni correction, depending on whether normality assumption was met). (**B**) Same as **A** but the average model accuracy is plotted separately for mice with (near-)complete and partial lesions. Dots at the top indicate the timepoints where the model performance was significantly different between partial vs (near-)complete mice (purple), (near-)complete vs non-lesioned mice (blue), and partial vs non-lesioned mice (red) ($p < 0.05$, one-sided Mann-Whitney U test or t-test with Bonferroni correction, depending on whether normality assumption was met). Shaded areas represent 95% confidence intervals.

Pre-stimulus activity is predictive of the upcoming trial outcome. Remarkably, decoding accuracy was better than baseline even before stimulus onset. This could reflect changes in the network state that led or contributed to the upcoming trial outcome. For instance, changes in arousal or motivation can alter both the probability that an upcoming stimulus is detected and the activity of neurons in the network (Lee and Dan, 2012, McGinley et al., 2015). The decoding models might detect such changes in activity, resulting in higher decoding accuracy prior to stimulus onset. Additionally, pre-stimulus differences in hit and miss trial activity could also reflect the anticipation of an upcoming stimulus (Ruth et al., 1974; Nienhuis and Olds,

1978; Metzger et al., 2006) and the resulting change in attentional state. Inter-trial intervals in our experiments were randomly drawn from a normal distribution with a mean and standard deviation of 8 s and 2 s, respectively, and a lower bound of 3 s. Nevertheless, spontaneous licks did not occur at random times during the peri-catch trial periods following hit trials. Instead, average lick rates approximated the inter-trial interval distribution (Figure 6 - figure supplement 2A-D), suggesting that mice learned to adapt their behavior to this distribution and anticipate the timing of upcoming stimuli (Figure 6 - figure supplement 2E,F). Assuming that successfully anticipating the timing of an upcoming stimulus confers a greater chance of detecting the stimulus, neurons whose activity reflects that anticipation might be expected to show differences in pre-trial activity between hit and miss trials that could be detected by a decoding model. Note that for the analysis illustrated in Figures 5 and 6, hit trials were excluded if there were any licks between -500 ms and +120 ms (the latter number representing the lower bound of the animals' lick-latency) relative to stimulus onset, suggesting that changes in pre-stimulus activity cannot be directly related to licking.

Discussion

Imaging auditory corticorecipient neurons in the dorsal shell of the IC in mice trained to perform a sound detection task revealed that the majority of neurons exhibited distinct activity profiles for hit and miss trials, implying that they encode information beyond just the physical attributes of the stimulus. Indeed, using logistic regression models to classify hit vs miss trials, we found that the animals' behavioral choice can be read out from these neurons with a high degree of accuracy. Surprisingly, neural activity profiles and the decoding performance were similar in mice in which the auditory cortex had been lesioned bilaterally, suggesting that the midbrain has, independently of the auditory cortex, access to a wealth of non-acoustic information, which may be sufficient to support sound detection behavior.

Auditory corticocollicular axons terminate predominantly in the shell of the IC (Stebbings et al., 2014; Bajo and King, 2013) and the strongest effects of cortical manipulations have been reported in this region (Nakamoto et al., 2008; Vila et al 2019; Blackwell et al., 2020). However, these effects can be subtle (Cruces-Solis et al., 2018; Vila et al., 2019) or undetectable, especially when optogenetic silencing is used (Blackwell et al., 2020). Because of this and uncertainties over exactly what proportion of neurons in the shell of the IC is innervated by the auditory cortex and even where the border lies with the underlying central nucleus (Barnstedt et al., 2015), we used an anterograde transsynaptic tagging approach (Zingg et al., 2017) to identify corticorecipient neurons. This therefore maximized the chances of revealing the contribution of descending cortical input to the response properties of these midbrain neurons.

Inferior colliculus neurons exhibit task-related activity

Our recordings from corticorecipient neurons in the IC are consistent with previous studies demonstrating that neural representations of behavioral variables can be found in the auditory midbrain (Ruth et al., 1974; Nienhuis and Olds, 1978; Metzger et al., 2006; Gruters and Groh, 2012; Chen and Song, 2019; Yang et al., 2020; Saderi et al., 2021, Franceschi and Barkat, 2021). In keeping with responses recorded in the auditory cortex (Francis et al., 2018; Franceschi et al., 2021) and IC (Chen and Song 2019; Yang et al., 2020; Franceschi et al., 2021) of behaving mice, we found that the activity of most neurons was facilitated and about a third were suppressed during the sound detection task. Overall, only a small minority of clusters (mostly cluster 3) in our dataset showed what could be characterized as largely behavior-invariant response profiles to the auditory stimulus. In contrast, a large number of

neurons were clearly driven by variables other than the stimulus itself. Their activity may represent the choice (to lick or not to lick) that an animal made, preparatory motor activity, corollary discharge or the reward and the somatosensory or gustatory feedback associated with its consumption, as well as modulation by the animal's cognitive and behavioral state. Due to the task structure used, for the most part, it was not possible to unambiguously assign activity profiles to a particular variable. Nevertheless, we can speculate that neurons with late transients, such as in cluster 5, are more likely to represent corollary discharge and signals associated with the consumption of the reward, while those with very short latency peaks, as in clusters 4 and 10, may represent the animals' choice and/or preparatory motor activity.

When engaged in the detection task, an animal's arousal or motivational state may vary spontaneously or as a result of changes in, for instance, thirst, time of day or time into a session. In addition, cognitive factors, such as expectations about the timing of an upcoming trial (Ruth et al., 1974; Nienhuis and Olds, 1978; Metzger et al., 2006), which mice may have derived by learning the shape of the inter-trial interval distribution, may lead to variations in arousal or attentional state. Pre-trial differences in activity as well as the above-chance decoding performance before trial onset likely reflect the joint impact of those state changes on the activity of IC corticorecipient neurons and detection sensitivity (McCormick et al., 2020).

Contribution of the auditory cortex to task-related activity in the midbrain

Given the massive corticofugal projections that exist within the auditory system (Bajo and King, 2013), we hypothesized that task-related activity in the IC might depend on descending inputs from the auditory cortex. To address this, we imaged corticorecipient IC neurons during the same sound detection task after removing the cortical input. Consistent with previous work in the auditory (O'Sullivan et al., 2019) and somatosensory systems (Hong et al., 2018), we found that transient optogenetic silencing of the auditory cortex impaired sound detection, whereas cortical lesions had no effect on detection behavior, with lesioned mice learning the task as quickly as non-lesioned animals and achieving the same level of performance. In order to determine whether the absence of auditory cortical input alters the activity of IC neurons during sound detection behavior, we therefore focused on mice with bilateral cortical lesions to avoid the potentially confounding effects that reduced detection sensitivity produced by transient cortical silencing might have on the activity of IC neurons. For the same reason, we opted against the more targeted approach of optogenetic silencing of corticocollicular axons. Furthermore, it would have been difficult to silence the entire corticocollicular projection and the higher light powers required for manipulating axons compared to somata would have risked transmitting light to the cortex or other corticofugal targets, potentially causing behavioral changes and/or sacrificing specificity. Locally silencing corticocollicular axons would also have left indirect transmission via the thalamus between the auditory cortex and IC intact and would have been very challenging to verify. Finally, it has been reported that using optogenetic silencing tools in axons can have unintended consequences (Wiegert et al., 2017).

In keeping with our findings, numerous studies (reviewed in e.g. Pickles, 1988; Buser and Imbert, 1992) have shown that simple auditory skills, including the ability of freely moving rats to detect sounds (Kelly, 1970), are unaffected by the removal of the auditory cortex. However, transient pharmacological silencing of the auditory cortex in freely moving rats (Talwar et al., 2001), as well as head-fixed mice (Li et al., 2017), completely abolishes sound detection. The time course of the effects produced by muscimol application (Talwar et al 2001) suggests that there is a relationship between the size of the behavioral deficit and the degree of cortical inactivation. Consequently, milder impairments may be produced by the optogenetic

approaches employed by us and others (Kato et al 2015; O'Sullivan et al., 2019) because of incomplete suppression of cortical activity. Alternatively, the larger behavioral effects reported following muscimol application may be due to diffusion of the drug to other brain structures, potentially including the IC. Although our results cannot speak directly to the question of whether the preservation of sound detection without auditory cortex reflects a rewiring or repurposing of circuits in the brain, this seems unlikely given that other studies have shown that trained mice achieve pre-lesion performance levels on simple auditory discrimination (Ceballo et al., 2019; O'Sullivan et al., 2019) or somatosensory detection (Hong et al., 2018) tasks suddenly and within 48 hours following cortical ablation.

Why then does transient inactivation produce behavioral deficits? One possibility is that disabling the auditory cortex impacts behavior not because it contributes necessary computations or information, but because of the sudden and disruptive removal of tonic excitation (Oberle et al., 2021) to downstream targets (Otchy et al., 2015) that are indispensable for successful sound detection. In this scenario, normal operation would resume once synaptic scaling (Keck et al., 2013) had homeostatically restored normal activity in these structures, a process that has been suggested to take up to 48 hours and is consistent with the time course of recovery after lesions (Ceballo et al., 2019; Hong et al., 2018). Alternatively, several circuits may redundantly support sound detection. Silencing the auditory cortex might then transiently impede sound detection until the relevant downstream decision and motor structures have updated their synaptic weights and/or processing has shifted to the other circuits. Two observations, however, argue against this possibility. First, removing one of several redundant structures should leave some residual function intact and not have the devastating effect that pharmacological cortical silencing achieves (Talwar et al., 2001, Li et a., 2017). Second, other circuits mediating the acousticomotor transformation required for successful sound detection behavior very likely incorporate subcortical auditory structures, including the auditory midbrain. Activity in the IC may trigger actions (Cassedey and Covey, 1996), such as licking, via its direct projections to the superior colliculus, pontine nuclei, the periaqueductal gray (Hufman and Henson, 1990, Wenstrup et al., 1994, Casseday and Covey, 1996; Xiong et al., 2015) and the striatum (Allen Mouse Brain Connectivity experiment 100141596) or indirectly via its projections to the auditory thalamus. If cortical lesioning results in a greater weight being placed on the activity in spared subcortical circuits for perceptual judgements, we would expect the accuracy with which trial-by-trial outcomes could be read out from IC neurons to be greater in mice without auditory cortex. However, that was not the case.

A difference was observed, however, for decoding the behavior of mice from IC activity in mice with (near-)complete vs only partial lesions of the auditory cortex. Somewhat counterintuitively, trial outcomes could be read out with lower accuracy from the mice with smaller lesions. That smaller lesions can have a more disruptive effect than larger, more complete, lesions has been observed before, in that the time it takes mice to learn a whisker-dependent sensory detection task is anticorrelated with the size of their somatosensory cortex lesion (Hong et al., 2018). While the complete destruction of a cortical area severs all its communication with downstream structures, a partial lesion may actually be more disruptive by eradicating normal local processing while at the same time leaving intact some tissue, especially in the deeper output layers, which continue to transmit what are now aberrant activity patterns. The difference in decoding accuracy that we observed in the IC could thus be a consequence of residual and now disruptive cortical input.

Our results show that behavioral variables are encoded by corticorecipient neurons in the dorsal shell of the IC independently of their main source of descending input, the auditory

464 cortex. It therefore seems likely that this region of the auditory midbrain is part of the circuit
465 that supports sound detection behavior in the absence of the auditory cortex. Nevertheless,
466 except for the regions immediately bordering the auditory cortex, corticocollicular neurons
467 located in other areas were left intact. These relatively sparse descending projections to the
468 IC, such as those originating from somatosensory cortical areas (Lohse et al., 2021; Lesicko
469 et al., 2016) may have contributed to the response profiles that we observed. Additional non-
470 acoustic sensory input can reach the IC via brainstem nuclei (Lesicko et al., 2016; Shore and
471 Zhou, 2006) and the superior colliculus (Chen et al., 2020; Coleman and Clerici, 1987). The
472 latter, together with input from the substantia nigra (Olazabal and Moore, 1989) and the globus
473 pallidus (Morizumi and Hattori, 1991) may also be a source of motor signals, while state
474 changes may impact on the IC via inputs from neuromodulatory structures, including the locus
475 coeruleus and the subparafascicular, dorsal raphe and tegmental nuclei (Chen et al., 2020,
476 Liu et al., 2023).

477 **Conclusion**

478 Behavior is a major determinant of activity in the non-lemniscal auditory midbrain and thus key
479 to understanding how it contributes to hearing. The anatomical feature that defines this
480 structure more than any others is its connection with the auditory cortex. While modulation of
481 IC activity by this descending projection has been implicated in various functions, most notably
482 in the plasticity of auditory processing, we have shown that the auditory cortex is not required
483 for the task-related activity recorded in IC neurons of mice performing a sound detection task.
484 These results therefore emphasize more than ever the need to factor in subcortical processing
485 when considering how the cortex contributes to sound-guided behavior.

486

487 **Materials and methods**

488 **Animals.** All experiments were approved by the Committee on Animal Care and Ethical
489 Review at the University of Oxford and were licensed by the UK Home Office (Animal Scientific
490 Procedures Act, 1986, amended in 2012). We used 22 (3 female, 19 male) Ai95 (RCL-
491 GCaMP6f)-D (JAX 024105, Jackson Laboratories, USA), three (one female, two male) Gad2-
492 IRES-Cre (JAX 010802, Jackson Laboratories, USA), six female Ai9 (RCL-tdT) (JAX 007909,
493 Jackson Laboratories, USA), two female Ai95 (RCL-GCaMP6f)-D X VGAT-cre (JAX 016962,
494 Jackson Laboratories, USA), three female Ai95 (RCL-GCaMP6f)-D X T29-1 (Camk2a-cre,
495 JAX 005359, Jackson Laboratories, USA) and three (one male, two female)
496 C57BL6/NTac.Cdh23 (MRC Harwell, UK) mice. All mice were 9–15 weeks old during data
497 collection. They were maintained on a 12-h light/dark cycle and were housed at 20–24°C with
498 a relative humidity of 45–65%.

499 **Surgeries.** For all surgical procedures, mice were premedicated with intraperitoneal injections
500 of dexamethasone (Dexadreson, 4 mg), atropine (Atrocare, 1 mg) and carprofen (Rimadyl,
501 0.15 mg) before being anesthetized with isoflurane (1.5-2%) and administered with
502 buprenorphine (Vetergesic, 1 ml/kg) postoperatively. Mice were then placed in a stereotaxic
503 frame (Model 900LS, David Kopf Instruments, CA, USA) and their body temperature was kept
504 constant at 37°C by the use of a heating mat and a DC temperature controller in conjunction
505 with a temperature probe (FHC, ME, USA).

506 For injections in the auditory cortex of AAV1.hSyn.Cre.WPRE (Penn Vector Core), the skin
507 over this part of the brain was shaved and an incision was made, after which three small holes
508 were drilled (Foredom K.1070, Blackstone Industries, CT, USA) into the skull with a 0.4 mm
509 drill bit and the virus injected using a pulled glass pipette and a custom pressure injection
510 system. In order to express GCaMP6f or tdTomato in IC neurons that receive auditory cortical
511 inputs, a total of 150-200 nl of AAV1.hSyn.Cre.WPRE was injected at three sites in the right
512 auditory cortex of GCaMP6f (Ai95D) or tdTomato (Ai9) reporter mice, respectively, at depths
513 of 450-550 µm below the brain surface. Given the anterograde transsynaptic spread properties
514 of AAV1 (Zingg et al. 2017), this caused the expression of the desired fluorescent protein in
515 structures that the auditory cortex projects to, including the shell of the IC (Figure 4A,B).

516 In order to prepare GAD2-Ires-Cre mice for the optogenetics experiments, we removed a large
517 flap of skin over the parietal and temporal bones, partially removed the temporal muscles and
518 performed a circular craniotomy of 3 mm diameter over each auditory cortex. We then injected
519 a total of 500 nl of AAV5-EF1a-DIO-hChR2-EYFP, UNC Vector Core) bilaterally across 4 sites
520 and two depths (200 and 600 µm) into the auditory cortex. Each craniotomy was covered with
521 a circular 3 mm glass window that was attached to the edges of the skull with cyanoacrylate
522 glue (Pattex Ultra Gel, Henkel), and the exposed skull was sealed with dental acrylic (C&B
523 Superbond, Sun Medical, Japan) into which a custom steel bar was embedded for head
524 fixation. Experiments commenced approximately three weeks afterwards.

525 The IC window implantation and cortical lesioning in the Ai95D mice were performed at least
526 three weeks after the injections. The window implantation involved removing a flap of skin over
527 the (inter-)parietal and occipital bone and making a circular 3 mm craniotomy over the
528 midbrain. A 3-mm diameter glass coverslip that had been glued to a ~1 mm tall steel cylinder
529 with 0.5 mm wall thickness was inserted into this craniotomy. The cylinder allowed us to press
530 the glass window gently onto the brain (in order to minimize brain movement during
531 experiments) and was then glued to the edges of the skull. For head fixation, we embedded a
532 custom steel plate in the dental acrylic used to seal the exposed bone.

533 Lesions were performed as part of the cranial window implantation surgery. In those mice
534 undergoing lesions, we removed a slightly larger flap of skin on both sides in order to expose
535 the temporal bone, detached and deflected and/or partly removed the temporal muscle and
536 then made, on both sides, an elliptical craniotomy over the auditory cortex of ~3 mm
537 (dorsoventral) by 4 mm (rostrocaudal). The exposed tissue was then aspirated (Hong et al .,
538 2018) with a blunted 19 G needle connected to a suction pump (Eschmann Vp25, UK) or
539 destroyed by thermocoagulation (Ceballo et al., 2019) with a cauterizer (Small Vessel
540 Cauterizer Kit, FST, Germany) and the piece of skull that had been removed for the craniotomy
541 was glued (Pattex Ultra Gel) back in place. In some of the lesioned mice, after completion of
542 the imaging, 150 nl of a retrograde viral construct (rAAV2-CAG-tdTomato, UNC Vector Core)
543 was injected into the dorsal IC across three sites at depths of 100-400 µm below the brain
544 surface in order to visualize the remaining IC-projecting cortical neurons. The extent of the
545 lesions was estimated from the histological sections and by referencing them against sections
546 from a mouse brain atlas (Paxinos and Franklin, 2001).

547 In order to visualize the distribution of IC-projecting neurons in mice without cortical lesions,
548 150 nl of the retrograde rAAV2-CAG-cre (UNC Vector Core) construct was injected into the

549 dorsal IC of one Ai9 mouse with an intact cortex across three sites at depths of 100-400 µm
550 below the brain surface.

551 **Histology.** For histological processing, mice were perfused transcardially, first with phosphate
552 buffered saline (PBS) and then with 4% paraformaldehyde in (PBS), and their brains were
553 sectioned coronally (100 µm thick) with a vibratome (Leica). Images were taken manually
554 using Leica DMR microscope, a confocal laser scanning microscope (Olympus FV1000) or
555 with an automated slide scanner (Zeiss Axioscan Z1). The brain of one mouse (Figure 2 -
556 figure supplement 1) was sectioned and imaged on a custom-built two-photon whole brain
557 tomograph.

558 **Click detection task.** Starting 2-3 days before training commenced, the mice were habituated
559 to head fixation in the experimental setup and their access to water was restricted to about ~1
560 ml per day, bringing their body weight down to about ~85% of the pre-restriction values. During
561 the training phase, the mice were required to report a 0.5 ms broadband click stimulus of 80
562 dB SPL by licking a water spout positioned in front of them. Licking within a 1.5-second
563 response window (occasionally this was reduced in duration to discourage excessive licking)
564 triggered an immediate water reward (~2 µl). Stimulus trials and catch (no stimulus) trials were
565 randomly interleaved with an inter-trial interval drawn from a normal distribution with a mean
566 and standard deviation of 8 s and 2 s, respectively, and a lower bound of 3 s. Successful
567 reporting of the sound within the response window was scored a 'hit', while failure to respond
568 was scored a 'miss'. During catch trials, neither licking ('false alarm') nor withholding licking
569 ('correct rejection') triggered a reward. To help the mice form an association between sound
570 and reward, they received occasional 'free' rewards in stimulus trials during the initial training
571 even when no licking occurred.

572 Once the mice had achieved a stable level of performance (typically two days with d' > 1.5),
573 quieter stimuli (41-71 dB SPL) were introduced. The range of sound levels was adjusted to
574 each animal's behavioral performance to avoid floor and ceiling effects and could, therefore,
575 differ from mouse to mouse. The behavioral experiments were run using custom MATLAB
576 (MathWorks) scripts interfacing with a National Instruments board (NI USB-6501) for reward
577 delivery and lick registration. The stimuli were presented using Psychtoolbox through a free-
578 field speaker (Vifa, Avisoft Bioacoustics, Germany), positioned about ~15 cm from the snout
579 of the mouse. Stimuli were calibrated using a Pettersson M500 microphone, which was itself
580 referenced to a sound-level calibrator (Iso-Tech SLC-1356). Stimulus levels were calibrated
581 by integrating the recorded RMS of clicks over the mouse hearing range (1-100 kHz) and
582 comparing this to the RMS of stimuli from the reference sound-level calibrator.

583 In the optogenetics experiments, the behavioral task was identical except that a single sound
584 level (80 dB SPL) was used and on 50% of the trials bilateral photostimulation (20 Hz, 10 ms
585 pulses, 0.2 mW/mm^2) was performed via two 470 nm LEDs (CREE-XP-E2, LED-Tech,
586 Germany) positioned above the cranial windows. LED-on and LED-off trials were randomly
587 interleaved and stimulation lasted for 700 ms starting 50 ms before trial onset. Furthermore,
588 masking flashes were presented on all trials from two bright LEDs (60 mW) positioned a few
589 cm in front of the animals' eyes.

590 **Two-photon calcium imaging.** Imaging was performed at a depth of 50 µm – 150 µm from
591 the IC surface using a commercial two-photon laser-scanning microscope (B-Scope,

ThorLabs, VA, USA), a SpectraPhysics Mai-Tai eHP laser (Spectra-Physics, CA, USA) tuned to 930 nm, and a Nikon 16x 0.8 NA objective. Images were acquired with a resolution of 512 by 512 pixels at a rate of ~28 Hz. The size of the field of view was either 500 μm by 500 μm or 666 μm by 666 μm, which allowed us to, typically, image dozens of corticorecipient IC neurons simultaneously. Each imaging session lasted around 1-2 hours.

Image processing. Rigid and non-rigid image registration, segmentation, neuropil correction and signal extraction were performed using the Python version of suite2p (Pachitariu et al. 2017). To assess the extent of image displacement in the z-axis, we compared the average of the top and the bottom 500 frames of each spatial principal component (PC) of the registered images for every 8-16 minutes of the recordings. Any region of interest (ROI) with substantial z-axis movement was excluded from further analysis. Sessions in which the majority of ROIs had to be excluded were discarded entirely. Furthermore, in order to specifically assess brain motion caused by the motor component of the task, i.e. the animal's licking, lick-triggered movies of the imaging frames were created for every 8-16 minutes of the recordings. The rationale here is that if licking causes a stereotypical displacement of the imaging plane, this will become apparent when image sequences are averaged across lick events. Specifically, non-registered image sequences surrounding (from 2 s before to 2 s after) lick events were used to produce averaged lick-triggered movies. These lick-triggered movies, as well as non-averaged sequences, were then visually inspected and ROIs were excluded from subsequent analysis if they were affected by substantial z-motion.

Clustering analysis. To identify sub-populations of neurons with distinct response profiles, a clustering analysis was performed using an approach very similar to that described in Namboodiri et al. (2019). For each neuron, the trial-averaged activity was obtained by averaging across all the sound levels presented in a given session separately for hit and miss trials (given the small number of catch trials, approximately one tenth of all trials, this analysis was restricted to stimulus trials only). Differences in the field of view size between sessions resulted in slight differences in frame rate and thus frame duration. Therefore, the activity traces were linearly interpolated to have the same number of data points (193 frames). For each neuron, the trial-averaged activity for miss trials was appended to that for hit trials, producing 386 data points per neuron for a total of 2649 neurons (n = 1697 neurons from 38 sessions with 9 non-lesioned mice; n = 952 neurons from 37 sessions with 7 lesioned mice). To reduce the dimensionality of this dataset before applying the clustering algorithm, we performed principal components analysis (PCA) along the time axis to capture the temporal response profile for each neuron. Guided by the 'elbow' point in a scree plot visualizing the fraction of variance explained by each PC, we decided to project the dataset to the lower dimensional subspace formed by the first 9 PCs.

Spectral clustering was used to cluster the resulting data. The affinity matrix was constructed by computing a graph of nearest neighbors. The hyperparameters of the clustering algorithm, including the number of nearest neighbors and the number of clusters, were optimized by a grid search to maximize the mean Silhouette Score for all samples. The Silhouette Score is a measure of the compactness of individual clusters (intra-cluster distance) and the separation amongst clusters (inter-cluster distance). For a given sample i that belongs to cluster C_I, the Silhouette Score is defined as:

$$s_i = \frac{(b_i - a_i)}{max(a_i, b_i)}$$

where a_i is the mean distance between sample i and all the other samples in the same cluster, and b_i is the mean distance of sample i to the nearest cluster that sample i is not part of. Let $|C_I|$ and $|C_J|$ be the number of samples belonging to clusters C_I and C_J, and $d(i,j)$ be the distance between samples i and j; a_i and b_i are defined as:

$$a_i = \frac{1}{|C_I| - 1} \sum_{j \in C_I, i \neq j} d(i,j)$$

$$b_i = \min_{J \neq I} \frac{1}{|C_J|} \sum_{j \in C_J} d(i,j)$$

The resulting clusters from the hyperparameter search were further examined by plotting clusters in pairs against each other with t-distributed Stochastic Neighbor Embedding, a statistical method for visualizing high-dimensional data that involves giving each data point a location in a two or three-dimensional space (van der Maaten and Hinton 2008), which showed that the clusters were generally separable.

Population decoding. Logistic regression models were trained on the network activity of each session to classify hit vs miss trials on a frame-by-frame basis, i.e., each time point (frame) of each session was trained separately. Sessions were only included if there were at least 15 instances for both hit and miss trials. The models were trained with L2 regularization, which gave similar contributions to correlated features (i.e., individual neuronal activity) instead of discarding some of the correlated features that were also related to behaviorally-relevant information. The strength of the regularization for each model was hyperparameter-tuned and the reported results were cross validated. Specifically, neuronal data in each session was split into 5 stratified folds, and each fold preserved the percentage of hit and miss trials in a given session. Four folds were used for cross-validated hyperparameter search (randomized search drawn from the log-uniform distribution between 1×10^{-4} and 1×10^{2}), and the remaining 1 fold was used for evaluating the model after the best hyperparameters were refitted on the 4 folds of data. To more reliably estimate the model results, the evaluation was done for each of the 5 folds for each session and the average of these 5 results was taken as each session's model performance at each timepoint.

The percentage of hit and miss trials was different in each session, and the number of hit trials often exceeded the number of miss trials. To include as many trials as possible while preventing the models from taking advantage of class imbalances, balancing procedures were performed at both the model-level and the metrics-level. First, logistic regression was trained with the class weights adjusted inversely proportional to the frequency of each trial type in the training data, giving higher weights to the minority class and lower weights to the majority class. Given the total number of trials in the training data N_T, the number of classes N_C, and the number of trials for a given class N_i, the weight for a given class W_i was defined as follows:

$$W_i = W_T \,/\, (N_C * N_i\ )$$

These weights were then applied to the cost function during the training process to increase the penalty for minority class misclassifications and reduce the penalty for majority class misclassifications. Second, to avoid the estimated model performance being inflated due to class imbalance, balanced accuracy (Brodersen et al. 2010) was used to report the model performance. Balanced accuracy was defined as the arithmetic mean of the true positive rate and the true negative rate. For a model performing equally well on either class, the balanced accuracy is the same as the conventional accuracy (i.e., the number of correct predictions divided by the total number of predictions). However, for a model scoring above chance only because the model takes advantage of the class imbalance (i.e. consistently predicts the majority class), the balanced accuracy is at chance level.

$$Balanced\ accuracy\ = \frac{1}{2} * \left(\frac{N_{true\ pos.}}{N_{true\ pos.}+N_{true\ neg.}} + \frac{N_{true\ neg.}}{N_{true\ neg.}+N_{true\ pos.}}\right)$$

Additionally, dummy models were used as baseline models to compare against the performance of the logistic regression models. Dummy models predicted the class labels (i.e., hit or miss trials) randomly while taking into account the probability of each class.

To assess whether the model performance was correlated with the number of ROIs recorded in a session, Spearman's correlation coefficient was computed between the number of ROIs in a session and the mean model performance over different 1-second time periods relative to stimulus onset (from 2 seconds before to 5 seconds after stimulus onset).

Statistical tests were conducted to compare the model performance between lesioned and non-lesioned mice, as well as between the trained models and dummy models. Since the frame rate varied slightly with the size of the field of view, the numbers of frames (193 - 197 frames) per 7-s trial could be different across sessions. Thus, model performance was linearly interpolated to make all sessions contain the same number of frames before statistical tests were performed at each timepoint. The model performance of each session was cross-validated and averaged across folds, and the statistical tests were performed on the distributions of the sessions' model performance. The Shapiro–Wilk test was used to determine whether a parametric or nonparametric test should be used, using $p < 0.05$ as a criterion. A one-sided Wilcoxon signed-rank test or paired t-test was performed for comparing trained vs dummy models, while a one-sided Mann-Whitney U test or t-test was performed for comparing trained models for different groups of mice. Because of the smaller sample sizes, the statistical tests in Figure 6B were carried out after binning the scores for every two timepoints. Statistical significance was defined as $p < 0.05$ after Bonferroni correction.

Data availability. Data will be made available in a public repository.

Acknowledgments. We are grateful to Christopher Breen and Robert Campbell for helping with the histology and for the financial assistance provided by an Oxford-Taiwan Graduate Scholarship from the University of Oxford and the Taiwan Ministry of Education to TYL, a Wellcome 4 year PhD Studentship to YW (102372/Z/13/Z), and by a Wellcome Principal Research Fellowship to AJK (WT108369/Z/2015/Z).

713 **References**

714 Antunes FM, Malmierca MS. 2021. Corticothalamic Pathways in Auditory Processing: Recent
715 Advances and Insights From Other Sensory Systems. Frontiers in Neural Circuits.
716 doi:10.3389/fncir.2021.721186

717 Bajo VM, King AJ. 2013. Cortical modulation of auditory processing in the midbrain. Frontiers
718 in Neural Circuits **6**:114. doi:10.3389/fncir.2012.00114

719 Barnstedt O, Keating P, Weissenberger Y, King AJ, Dahmen JC. 2015. Functional
720 Microarchitecture of the Mouse Dorsal Inferior Colliculus Revealed through In Vivo Two-
721 Photon Calcium Imaging. Journal of Neuroscience **35**:10927–10939.
722 doi:10.1523/JNEUROSCI.0103-15.2015

723 Blackwell JM, Lesicko AM, Rao W, De Biasi M, Geffen MN. 2020. Auditory cortex shapes
724 sound responses in the inferior colliculus. eLife. doi:10.7554/elife.51890

725 Brodersen KH, Ong CS, Stephan KE, Buhmann JM. 2010. The Balanced Accuracy and Its
726 Posterior Distribution. doi:10.1109/icpr.2010.764

727 Buser PA, Imbert M. 1992. Audition. Cambridge, Mass.: MIT Press.

728 Casseday JH, Covey E. 1996. A neuroethological theory of the operation of the inferior
729 colliculus. Brain, behavior and evolution **47**:311–336. doi:10.1159/000113249

730 Ceballo S, Piwkowska Z, Bourg J, Daret A, Bathellier B. 2019. Targeted Cortical Manipulation
731 of Auditory Perception. Neuron **104**:1168-1179.e5. doi:10.1016/j.neuron.2019.09.043

732 Chen C, Song S. 2019. Differential cell-type dependent brain state modulations of sensory
733 representations in the non-lemniscal mouse inferior colliculus. Communications Biology **2**:356.
734 doi:10.1038/s42003-019-0602-4

735 Chen CC, Cheng MM, Ito T, Song SS. 2018. Neuronal Organization in the Inferior Colliculus
736 Revisited with Cell-Type-Dependent Monosynaptic Tracing. The Journal of Neuroscience.
737 doi:10.1523/jneurosci.2173-17.2018

738 Coleman JR, Clerici WJ. 1987. Sources of projections to subdivisions of the inferior colliculus
739 in the rat. Journal of comparative neurology (1911) **262**:215–226. doi:10.1002/cne.902620204

740 Cruces-Solís H, Jing Z, Babaev O, Rubin J, Gür B, Krueger-Burg D, Strenzke N, De Hoz L.
741 2018a. Auditory midbrain coding of statistical learning that results from discontinuous sensory
742 stimulation. PLOS Biology. doi:10.1371/journal.pbio.2005114

743 De Franceschi G, Barkat TR. 2021. Task-induced modulations of neuronal activity along the
744 auditory pathway. Cell reports (Cambridge) **37**:110115. doi:10.1016/j.celrep.2021.110115

745 Engel AK, Fries P, Singer W. 2001. Dynamic predictions: oscillations and synchrony in top-
746 down processing. Nature reviews. Neuroscience **2**:704–716. doi:10.1038/35094565

747 Francis NA, Winkowski DE, Sheikhattar A, Armengol K, Babadi B, Kanold PO. 2018. Small
748 Networks Encode Decision-Making in Primary Auditory Cortex. Neuron (Cambridge, Mass.)
749 **97**:885-897.e6. doi:10.1016/j.neuron.2018.01.019

750 Hong YK, Lacefield CO, Rodgers CC, Bruno RM. 2018. Sensation, movement and learning in
751 the absence of barrel cortex. Nature **561**:542–546. doi:10.1038/s41586-018-0527-y

752 Huffman RF, Henson OW. 1990. The descending auditory pathway and acousticomotor
753 systems: connections with the inferior colliculus. Brain Research Reviews **15**:295–323.
754 doi:10.1016/0165-0173(90)90005-9

755 Kato HK, Gillet SN, Isaacson JS. 2015. Flexible Sensory Representations in Auditory Cortex
756 Driven by Behavioral Relevance. Neuron **88**:1027–1039. doi:10.1016/j.neuron.2015.10.024

757 Keck T, Keller GB, Jacobsen RI, Eysel UT, Bonhoeffer T, Hübener M. 2013. Synaptic Scaling
758 and Homeostatic Plasticity in the Mouse Visual Cortex In Vivo. NEURON **80**:327–334.
759 doi:10.1016/j.neuron.2013.08.018

760 Kelly, Buzzard Jack. 1970. The effects of lateral lemniscal and neocortical lesions on auditory
761 absolute thresholds and frequency difference thresholds of the rat . Vanderbilt.

762 King AJ, Bajo VM, Nodal FR, Moore DR. 2010. The descending corticocollicular pathway
763 mediates learning-induced auditory plasticity. Nature neuroscience **13**:253–260.
764 doi:10.1038/nn.2466

765 Kraus N, White-Schwoch T. 2015. Unraveling the Biology of Auditory Learning: A Cognitive–
766 Sensorimotor–Reward Framework. Trends in cognitive sciences **19**:642–654.
767 doi:10.1016/j.tics.2015.08.017

768 Lee S-H, Dan Y. 2012. Neuromodulation of Brain States. Neuron **76**:209–222.
769 doi:10.1016/j.neuron.2012.09.012

770 Lesicko AMH, Hristova TS, Maigler KC, Llano DA. 2016. Connectional Modularity of Top-
771 Down and Bottom-Up Multimodal Inputs to the Lateral Cortex of the Mouse Inferior Colliculus.
772 The Journal of Neuroscience. doi:10.1523/jneurosci.4134-15.2016

773 Li J, Liao X, Zhang Jianxiong, Wang M, Yang N, Zhang Jun, Lv G, Li H, Lu J, Ding R, Li X,
774 Guang Y, Yang Z, Qin H, Jin W, Zhang K, He C, Jia H, Zeng S, Hu Z, Nelken I, Chen X. 2017.
775 Primary Auditory Cortex is Required for Anticipatory Motor Response. Cerebral Cortex.
776 doi:10.1093/cercor/bhx079

777 Liu M, Xie F, Dai J, Zhang J, Yuan K, Wang N. 2023. Brain-wide inputs to the non-lemniscal
778 inferior colliculus in mice. Neuroscience letters **793**:136976. doi:10.1016/j.neulet.2022.136976

Lohse M, Bajo VM, King AJ, Willmore BDB. 2020. Neural circuits underlying auditory contrast gain control and their perceptual implications. Nature Communications **11**:324. doi:10.1038/s41467-019-14163-5

Malmierca MS, Anderson LA, Antunes FM. 2015. The cortical modulation of stimulus-specific adaptation in the auditory midbrain and thalamus: a potential neuronal correlate for predictive coding. Frontiers in systems neuroscience **9**:19. doi:10.3389/fnsys.2015.00019

Mccormick DA, Nestvogel DB, He BJ. n.d. Neuromodulation of Brain State and Behavior. doi:10.1146/annurev-neuro-100219-

McGinley MJ, Vinck M, Reimer J, Batista-Brito R, Zagha E, Cadwell CR, Tolias AS, Cardin JA, McCormick DA. 2015. Waking State: Rapid Variations Modulate Neural and Behavioral Responses. Neuron **87**:1143–1161. doi:10.1016/j.neuron.2015.09.012

Mettler FA. 1935. Corticifugal fiber connections of the cortex of Macaca mulatta. The temporal region. Journal of comparative neurology (1911) **63**:25–47. doi:10.1002/cne.900630104

Metzger RR, Greene NT, Porter KK, Groh JM. 2006. Effects of Reward and Behavioral Context on Neural Activity in the Primate Inferior Colliculus. The Journal of neuroscience **26**:7468–7476. doi:10.1523/JNEUROSCI.5401-05.2006

Moriizumi T, Hattori T. 1991. Pallidotectal projection to the inferior colliculus of the rat. Experimental brain research **87**:223–226. doi:10.1007/BF00228524

Musall S, Kaufman MT, Juavinett AL, Gluf S, Churchland AK. 2019. Single-trial neural dynamics are dominated by richly varied movements. Nature Neuroscience. doi:10.1038/s41593-019-0502-4

Nakamoto KT, Jones SJ, Palmer AR. 2008. Descending Projections From Auditory Cortex Modulate Sensitivity in the Midbrain to Cues for Spatial Position. Journal of Neurophysiology **99**:2347–2356. doi:10.1152/jn.01326.2007

803 Namboodiri VMK, Otis JM, Van Heeswijk K, Voets ES, Alghorazi RA, Rodriguez-Romaguera
804 J, Mihalas S, Stuber GD. 2019. Single-cell activity tracking reveals that orbitofrontal neurons
805 acquire and maintain a long-term memory to guide behavioral adaptation. Nature
806 Neuroscience. doi:10.1038/s41593-019-0408-1

807 Nienhuis R, Olds J. 1978. Changes in unit responses to tones after food reinforcement in the
808 auditory pathway of the rat: Intertrial arousal. Experimental Neurology. doi:10.1016/0014-
809 4886(78)90152-8

810 Noudoost B, Chang MH, Steinmetz NA, Moore T. 2010. Top-down control of visual attention.
811 Current opinion in neurobiology **20**:183–190. doi:10.1016/j.conb.2010.02.003

812 Oberle HM, Ford AN, Dileepkumar D, Czarny J, Apostolides PF. 2022a. Synaptic mechanisms
813 of top-down control in the non-lemniscal inferior colliculus. eLife. doi:10.7554/elife.72730

814 Olaźbal UE, Moore JK. 1989. Nigrotectal projection to the inferior colliculus: Horseradish
815 peroxidase transport and tyrosine hydroxylase immunohistochemical studies in rats, cats, and
816 bats. Journal of comparative neurology (1911) **282**:98–118. doi:10.1002/cne.902820108

817 O'sullivan C, Weible AP, Wehr M. 2019. Auditory Cortex Contributes to Discrimination of Pure
818 Tones. eneuro. doi:10.1523/eneuro.0340-19.2019

819 Otchy TM, Wolff SBE, Rhee JY, Pehlevan C, Kawai R, Kempf A, Gobes SMH, Ölveczky BP.
820 2015. Acute off-target effects of neural circuit manipulations. Nature. doi:10.1038/nature16442

821 Pachitariu M, Stringer C, Dipoppa M, der SS, Rossi L, Dalgleish H, Carandini M, Harris K.
822 2017. Suite2p: beyond 10,000 neurons with standard two-photon microscopy, bioRxiv. Cold
823 Spring Harbor: Cold Spring Harbor Laboratory Press. doi:10.1101/061507

824 Parker PRL, Brown MA, Smear MC, Niell CM. 2020. Movement-Related Signals in Sensory
825 Areas: Roles in Natural Behavior. Trends in neurosciences (Regular ed.) **43**:581–595.
826 doi:10.1016/j.tins.2020.05.005

827 Parras GG, Nieto-Diego J, Carbajal GV, Valdés-Baizabal C, Escera C, Malmierca MS. 2017.
828 Neurons along the auditory pathway exhibit a hierarchical organization of prediction error.
829 Nature Communications. doi:10.1038/s41467-017-02038-6

830 Paxinos G, Franklin KBJ, Franklin KBJ. 2001. The mouse brain in stereotaxic coordinates.
831 San Diego: Academic Press.

832 Pickles JO. 1988. An introduction to the physiology of hearing. London ; San Diego: Academic
833 Press.

834 Ruth RE, Peter Rosenfeld J, Harris DM, Birkel P. 1974. Effects of aversive and rewarding
835 electrical brain stimulation on auditory evoked responses in albino rat tectum. Physiology
836 & Behavior. doi:10.1016/0031-9384(74)90254-6

837 Saderi D, Schwartz ZP, Heller CR, Pennington JR, David SV. 2021. Dissociation of task
838 engagement and arousal effects in auditory cortex and midbrain. eLife.
839 doi:10.7554/elife.60153

840 Schneider DM, Mooney R. n.d. Annual Review of Neuroscience How Movement Modulates
841 Hearing. doi:10.1146/annurev-neuro-072116-

842 Schneider DM, Nelson A, Mooney R. 2014. A synaptic and circuit basis for corollary discharge
843 in the auditory cortex. Nature **513**:189–194. doi:10.1038/nature13724

844 Sherman SM. 2007. The thalamus is more than just a relay. Current opinion in neurobiology
845 **17**:417–422. doi:10.1016/j.conb.2007.07.003

846 Shore SE, Zhou J. 2006. Somatosensory influence on the cochlear nucleus and beyond.
847 Hearing research **216**:90–99. doi:10.1016/j.heares.2006.01.006

848 Singla S, Dempsey C, Warren R, Enikolopov AG, Sawtell NB. 2017. A cerebellum-like circuit
849 in the auditory system cancels responses to self-generated sounds. Nature neuroscience
850 **20**:943–950. doi:10.1038/nn.4567

851 Song Y-H, Kim J-H, Jeong H-W, Choi I, Jeong D, Kim K, Lee S-H. 2017. A Neural Circuit for
852 Auditory Dominance over Visual Perception. Neuron (Cambridge, Mass.) **93**:940-954.e6.
853 doi:10.1016/j.neuron.2017.01.006

854 Stebbings KA, Lesicko AMH, Llano DA. 2014. The auditory corticocollicular system: Molecular
855 and circuit-level considerations. Hearing research **314**:51–59.
856 doi:10.1016/j.heares.2014.05.004

857 Stringer C, Pachitariu M, Steinmetz N, Reddy CB, Carandini M, Harris KD. 2019. Spontaneous
858 behaviors drive multidimensional, brainwide activity. Science. doi:10.1126/science.aav7893

859 Suga N. 2008. Role of corticofugal feedback in hearing. Journal of Comparative Physiology
860 **194**:169–183. doi:10.1007/s00359-007-0274-2

861 Talwar SK, Musial PG, Gerstein GL. 2001. Role of Mammalian Auditory Cortex in the
862 Perception of Elementary Sound Properties. Journal of Neurophysiology **85**:2350–2358.
863 doi:10.1152/jn.2001.85.6.2350

864 van der Maaten L, Hinton G. 2008. Visualizing Data using t-SNE Laurens van der Maaten.
865 Journal of Machine Learning Research.

866 Vila C-H, Williamson RS, Hancock KE, Polley DB. 2019. Optimizing optogenetic stimulation
867 protocols in auditory corticofugal neurons based on closed-loop spike feedback. Journal of
868 Neural Engineering. doi:10.1088/1741-2552/ab39cf

869 Wenstrup JJ, Larue DT, Winer JA. 1994. Projections of physiologically defined subdivisions of
870 the inferior colliculus in the mustacbed bat: Targets in the medial geniculate body and

extrathalamic nuclei. Journal of comparative neurology (1911) **346**:207–236. doi:10.1002/cne.903460204

Wiegert JS, Mahn M, Prigge M, Printz Y, Yizhar O. 2017. Silencing Neurons: Tools, Applications, and Experimental Constraints. Neuron **95**:504–529. doi:10.1016/j.neuron.2017.06.050

Winer JA. 2005. Decoding the auditory corticofugal systems. Hearing research **207**:1–9. doi:10.1016/j.heares.2005.06.007

Xiong XR, Liang F, Zingg B, Ji X, Ibrahim LA, Tao HW, Zhang LI. 2015. Auditory cortex controls sound-driven innate defense behaviour through corticofugal projections to inferior colliculus. Nature Communications **6**:7224. doi:10.1038/ncomms8224

Yang Y, Lee J, Kim G. 2020. Integration of locomotion and auditory signals in the mouse inferior colliculus. eLife. doi:10.7554/elife.52228

Zingg B, Chou X, Zhang Z, Mesik L, Liang F, Tao HW, Zhang LI. 2017. AAV-Mediated Anterograde Transsynaptic Tagging: Mapping Corticocollicular Input-Defined Neural Pathways for Defense Behaviors. Neuron (Cambridge, Mass.) **93**:33–47. doi:10.1016/j.neuron.2016.11.045

Figure supplements

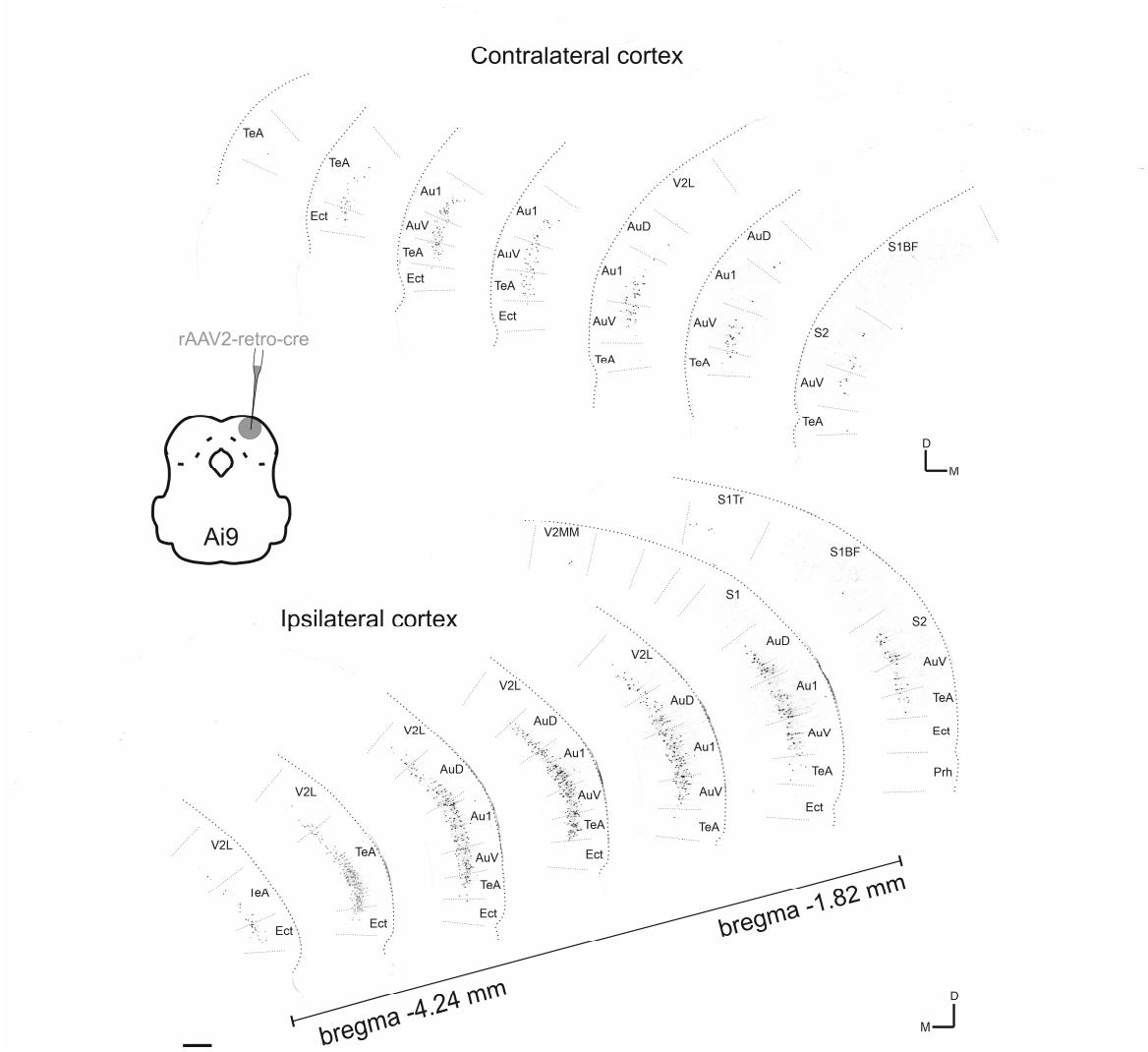

Figure 2 - figure supplement 1. Contra- and ipsilateral corticocollicular neurons along the rostrocaudal axis. Seven coronal sections are shown from each hemisphere covering approximately 2.5 mm of the rostrocaudal axis. Corticocollicular neurons were labeled by injecting a total of 150 nL of rAAV2-CAG-cre into the dorsal IC (at three sites and several depths from 100 µm - 400 µm below the brain surface) of a tdTomato reporter mouse (Ai9). Data were obtained using whole-brain laser scanning two-photon tomography. The resulting images were grayscale inverted and thresholded to remove all background labeling so that they could be more easily arranged into a common figure. Area borders were drawn onto the images according to Paxinos and Franklin (2001). Cortical area abbreviations: Au1, primary auditory; AuD, secondary auditory, dorsal; AuV, secondary auditory, ventral; Ect, ectorhinal; Prh, perirhinal; S1, primary somatosensory; S1BF, primary somatosensory, barrel field; S1Tr, primary somatosensory, trunk region; S2, secondary somatosensory; TeA, temporal association; V2L, secondary visual, lateral. Scale bar, 200 µm.

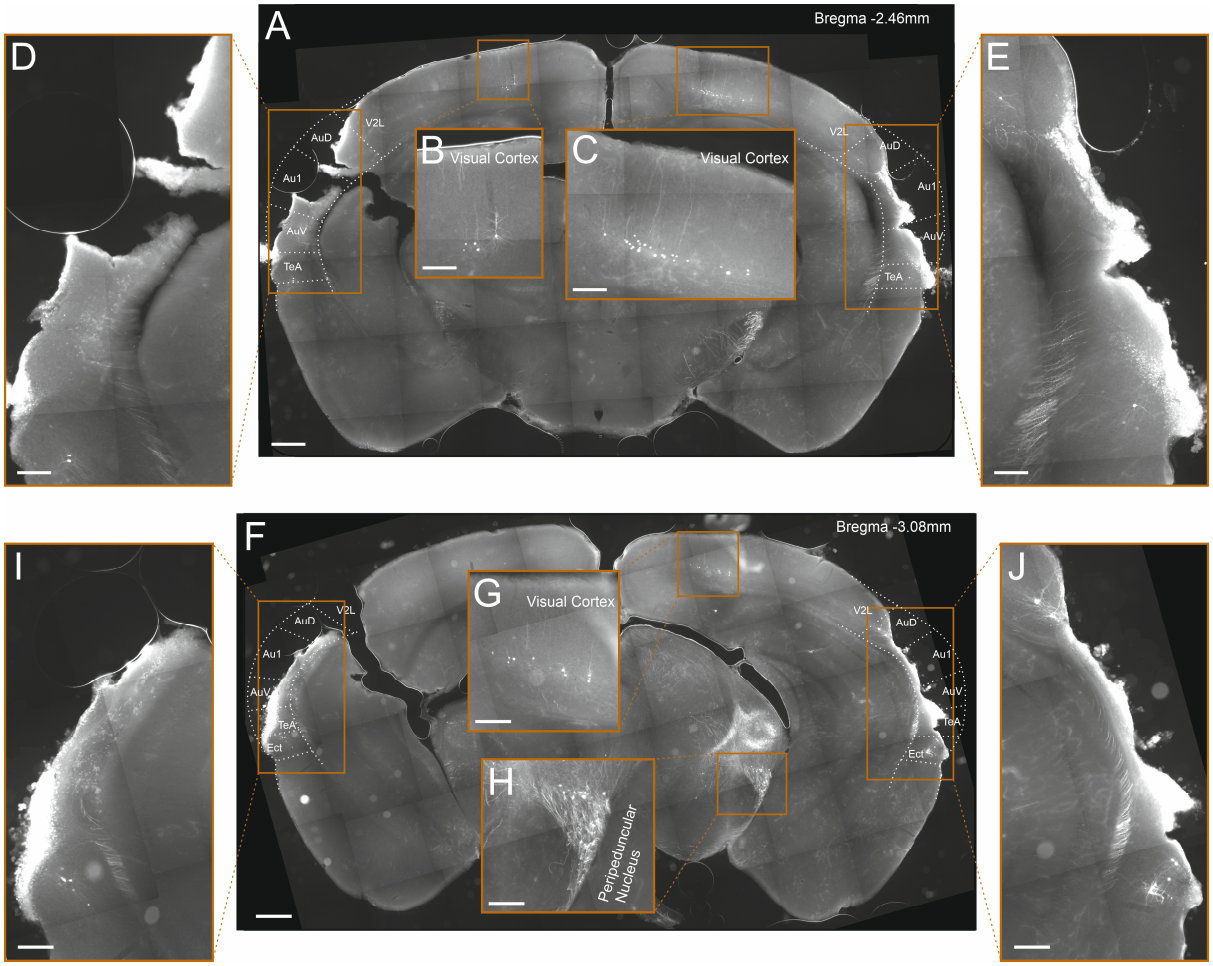

Figure 2 - figure supplement 2. Lesioning by thermocoagulation. (**A**) Coronal section showing lesion extent in a mouse that had undergone lesioning by thermocoagulation. After data collection had been completed, rAAV2-retro-tdTomato was injected along the dorsal IC in order to label corticocollicular neurons that had remained intact. Area borders were drawn onto the images according to Paxinos and Franklin (2001). Scale bar, 500 µm. (**B**,**C**) Higher magnification images showing tdTomato-labeled corticocollicular neurons in the left and right visual cortex. Scale bars, 200 µm. (**D**,**E)** Higher magnification images of the temporal regions surrounding the lesion sites, showing a very small number of residual corticocollicular neurons in the left and right temporal association area and the right dorsal auditory field. Scale bars, 200 µm. (**F)** Same as **A** for a different coronal section of the same mouse. (**G**,**H**) Higher magnification images showing tdTomato-labeled corticocollicular neurons in the right visual cortex and thalamocollicular neurons in the right peripeduncular nucleus. Scale bars, 200 µm. (**I**,**J)** Higher magnification images of the temporal regions surrounding the lesion sites showing a very small number of residual corticocollicular neurons in the left and right ectorhinal cortex and the right dorsal auditory field. Scale bars, 200 µm. While the lesion procedure spared some auditory cortex tissue in this animal, its visual appearance and the fact that barely any corticocollicular neurons could be found suggests that this residual tissue was almost completely destroyed. Consequently, we categorized this animal as having a (near-)complete lesion, meaning that 5% or less of the auditory cortex was left intact.

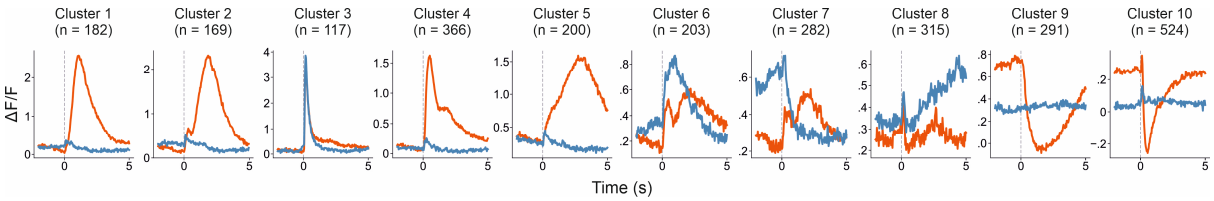

Figure 5 - figure supplement 1. Rescaled response profiles for each cluster. Averaged response profiles obtained by taking the mean across all neurons in a cluster separately for hit (red) and miss (blue) trials. Same as Figure 5B except that here each panel has an individualized y-axis range.

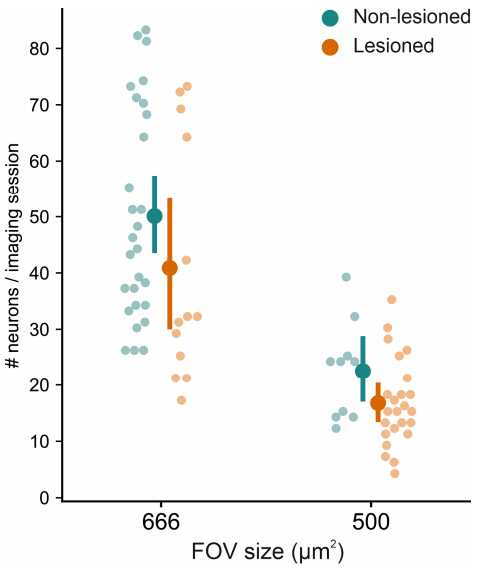

Figure 5 - figure supplement 2. Number of sessions for each imaging field of view size. A greater number of recordings happened to be made with the larger field of view in non-lesioned (28 of 38) than in lesioned (13 of 37) mice. Consequently, the number of neurons recorded in non-lesioned mice was greater than that recorded in lesioned mice (1697 vs 952). Error bars represent 95% confidence intervals.

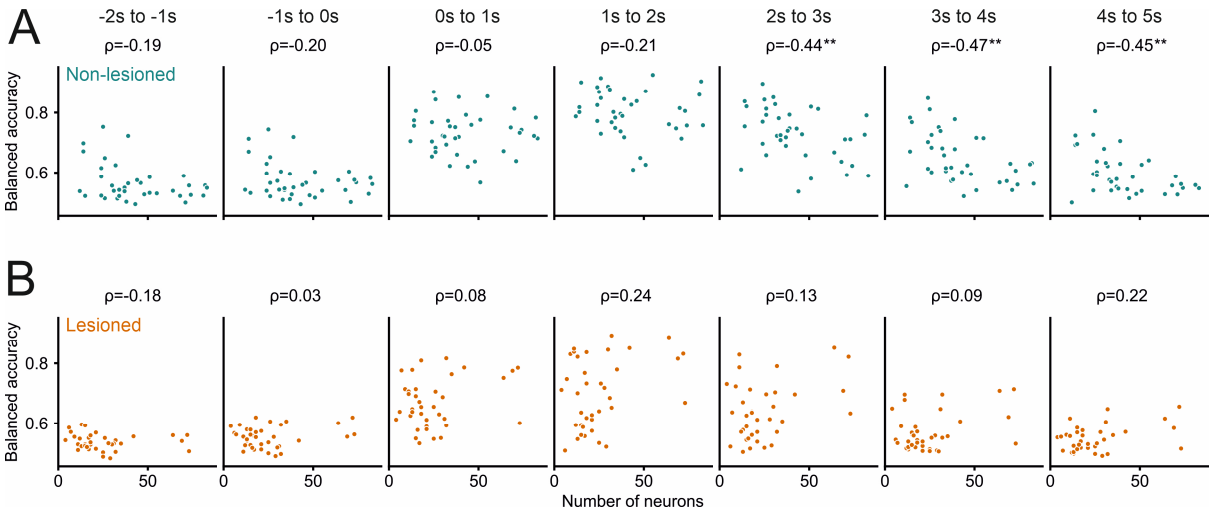

Figure 6 - figure supplement 1. Greater number of recorded neurons was not associated with better decoding performance. **(A,B)** Decoding performance (balanced accuracy) of the logistic regression models averaged over different 1-s time periods relative to stimulus onset as a function of the number of neurons recorded in a given session. A greater number of neurons obtained in a field of view was not associated with better decoding performance. Values above panels indicate Spearman's rank correlation coefficient ρ. The only statistically significant relationship between the number of recorded neurons and decoding performance was found for late trial periods in non-lesioned mice (A), and indicated that for time periods >2 seconds after stimulus onset a smaller sample size was associated with better decoding performance. **: $p < 0.01$.

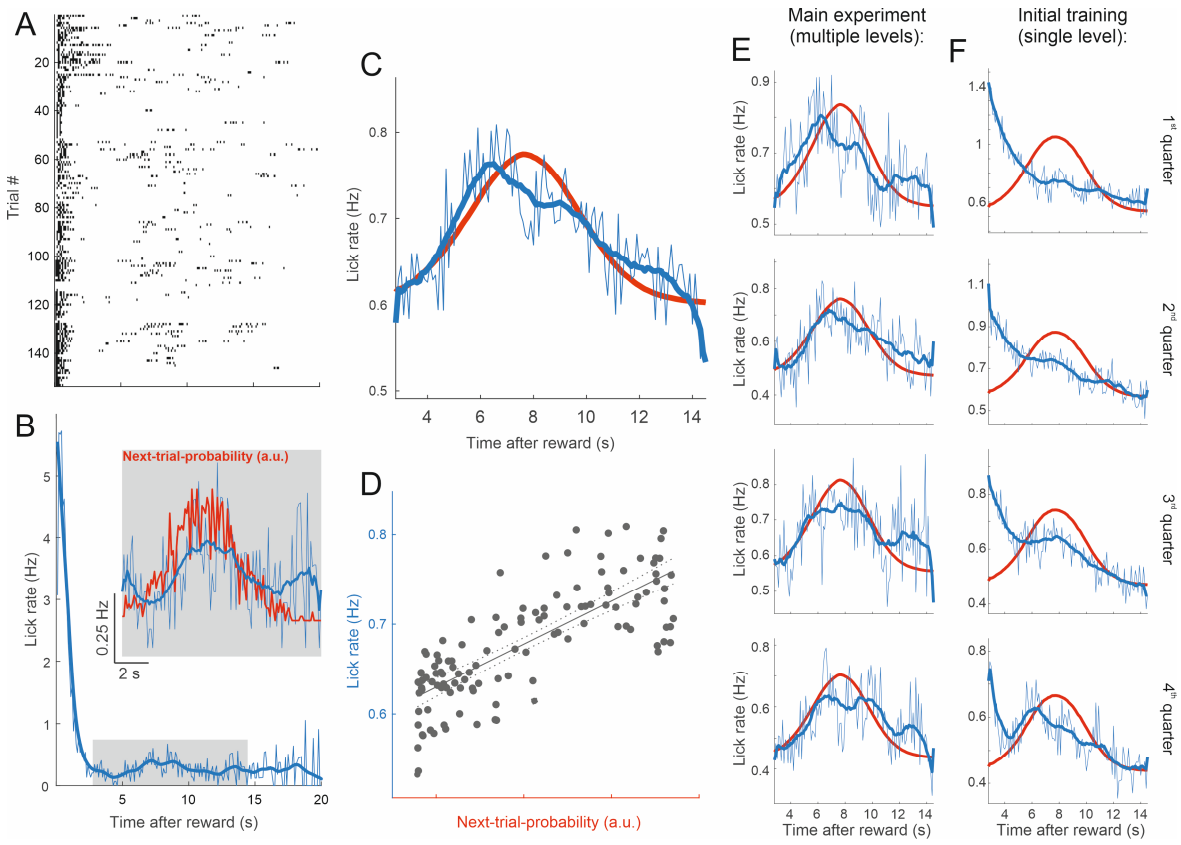

Figure 6 - figure supplement 2. Lick rates in peri-catch trial periods approximate next-trial-probability. (**A**) Peri-catch trial lick raster for all catch trials that followed a hit trial for one example mouse. The peri-catch trial period was defined as the period from the reward delivery in the hit trial to the onset of the trial following the catch trial. (**B**) Lick rate averaged across the peri-catch trial periods shown in **A** and binned into 100ms wide bins. The thick blue line shows the smoothed (20-point running average) lick rate. The inset gives a magnified view of the average lick rate during the period indicated by the gray rectangle. The red line illustrates the distribution of 'reward-to-next-trial-onset' intervals experienced by the example mouse. Given that licks are plotted time-locked to reward delivery, we plotted the distribution of intervals between reward delivery and onset of the next trial rather than the ITI distribution. In practice the difference between the two is roughly the latency between the stimulus and the first lick and thus barely distinguishable at this scale. As the distribution indicates the probability of the next trial presentation as a function of time since the preceding reward delivery we refer to it as 'next-trial-probability'. (**C**) Same as inset in **B** averaged across all mice. Next-trial-probability was smoothed with a 20-point running average. (**D**) Next-trial-probability as a predictor of lick rate. The dotted lines indicate the 95% confidence bounds around the regression fit. Adjusted $R^2 = 0.59$. Although the next-trial-probability is a good predictor of changes in the average lick rate, the lick rate at the peak of the distribution is merely about a quarter higher than at its tails where next-trial-probability approaches zero. Furthermore, to put the average lick rates into perspective, note that mice tend to lick in bouts, typically consisting of two to six licks in very quick succession (see lick raster in **A**), and that, consequently, the lick rate exceeds the underlying bout rate by a factor of about four. (**E**) Same as **C** but with peri-catch trials binned into four quarters before averaging in order to illustrate changes in lick behavior across different stages of the experiment. (**F**) Same as **E** for all peri-catch trials during the initial training with a single-level stimulus. While the peri-catch trial lick rate profile changed substantially over the course of the initial training (**F**) and started to approximate the stimulus probability distribution towards the end of training, it remained broadly stable throughout the main experiment (**E**). In order to increase the statistical power for this analysis, we included data from several additional mice used in other projects. These additional mice received the same training and performed the same task, but differed from those in the main dataset in that they had a different genetic background and/or had been fitted with a cranial implant for cortical rather than midbrain imaging. N for panels **C-F** = 34 mice.